Charge-to-spin conversion in twisted math xmlns="http://www.w3.org/1998/Math/MathML">mi>graphene/mi>mo>//mo>msub>mi>WSe/mi>mn>2/mn>/msub>/math> heterostructures

Seungjun Lee, D. J. P. de Sousa, Young-Kyun Kwon, Fernando de Juan, Zhendong Chi, Fèlix Casanova, and Tony Low

Phys. Rev. B **106**, 165420 — Published 20 October 2022

DOI: 10.1103/PhysRevB.106.165420

Charge-to-spin conversion in twisted graphene/WSe_2 heterostructures

Seungjun Lee,[1,*] D. J. P. de Sousa,[1,*] Young-Kyun Kwon,[2] Fernando de Juan,[3,4] Zhendong Chi,[5] Fèlix Casanova,[5] and Tony Low[1,6,†]

[1]*Department of Electrical and Computer Engineering, University of Minnesota, Minneapolis, Minnesota 55455, USA*
[2]*Department of Physics, Department of Information Display, and Research Institute for Basic Sciences, Kyung Hee University, Seoul, 02447, Korea*
[3]*Donostia International Physics Center, P. Manuel de Lardizabal 4, 20018 Donostia-San Sebastian, Spain*
[4]*IKERBASQUE, Basque Foundation for Science, Maria Diaz de Haro 3, 48013 Bilbao, Spain*
[5]*CIC nanoGUNE, 20018, Donostia-San Sebastián, Basque Country, Spain*
[6]*Department of Physics, University of Minnesota, Minneapolis, Minnesota 55455, USA*

(Dated: October 7, 2022)

We investigate the twist angle dependence of spin-orbit coupling proximity effects and charge-to-spin conversion (CSC) in graphene/WSe_2 heterostructures from first principles. The CSC is shown to strongly depend on the twist angle, with standard Rashba-Edelstein efficiency optimized near 30° twisting. Symmetry breaking due to twisting also gives rise to an unconventional Rashba-Edelstein effect, with electrically generated non-equilibrium spin densities possessing spins collinear to the applied electric field. Our work provides a new perspective on the electrical generation of spins in van der Waals heterostructures.

Graphene is an attractive channel material for spintronics owing to its long room-temperature spin diffusion length [1–4] and high carrier mobility [5, 6]. However, its applicability is also strongly limited by its weak intrinsic spin-orbit coupling (SOC), which impacts the generation and manipulation of spin currents [3]. Recent studies have established that proximity effects can significantly enhance SOC in graphene overlaid on transition metal dichalcogenides (TMDC) [7–11]. Here, the Dirac states in graphene inherit distinctive spin-textures from the proximity-induced valley-Zeeman and Rashba SOC, which gives rise to interesting phenomena such as weak anti-localization [12–16], giant spin lifetime anisotropy [17–19] and SOC-induced spin precession [20]. Transport measurements have unambiguously demonstrated efficient charge-to-spin conversion (CSC) in proximitized graphene, which can be attributed to either spin Hall or Rashba-Edelstein effects (SHE and REE, respectively) [21–25].

Spin signals produced by SHE and REE can be differentiated through the direction of their generated spin polarization, which are enforced by symmetry to be mutually orthogonal to each other and transverse to the applied electric field direction [24]. Twisted graphene/TMDC heterostructures are macroscopic chiral objects, mediated by the quantum interlayer coupling between the layers. The chirality implies that all mirror symmetries are broken, thus lifting the constraint on the allowed electrically generated spin polarization direction. Recent theoretical studies have suggested that SOC proximity effects are sensitive to the twist angle between graphene and TMDC [26–31]. However, little is known about the impact of twist angle on the CSC, in conjunction to the allowed new spin current components in this low symmetry chiral configuration.

In this letter, we address the twist angle dependence of SOC proximity effects and its connection to CSC in graphene/WSe_2 heterostructures by means of first principles calculations. We discovered the existence of an unconventional REE (UREE), where the spin density polarization is collinear with the applied electric field direction. Our results indicate that CSC is generally sensitive to the twist angle, with standard REE efficiency being maximized around the 30° twist angle. Our work provides a first principles-based account for CSC in twisted van der Waals heterostructures.

We performed first-principles calculations based on the density functional theory (DFT) [32, 33] for a total of 8 twisted graphene/WSe_2 heterostructures constructed using the coincidence lattice method [34, 35]. Our lattice alignment convention is shown in Figs. 1(a) and (b), where the $\theta = 0°$ ($\theta = 30°$) twisted heterostructure is such that the zigzag direction of graphene layer is aligned with the zigzag (armchair) direction of the WSe_2 lattice. It is noteworthy that the unavoidable strain originating from the artificial commensurate supercell structures can alter the relative band alignment between the graphene and the TMDC [36] and the SOC strength imprinted on graphene [28, 34]. Therefore, we carefully chose the size of the supercell structures to allow only for strain value of less than 2% for all structures. For more detailed description of DFT calculations [32, 33], see Supplementary Information (SI) [37]. In all twist angles, the Dirac cones of graphene lie within the WSe_2 band gap, which guarantees that charge and spin transport in twisted graphene/WSe_2 is Dirac-like at low dopings [11, 38]. (See also Fig.S2)

We now analyse the proximity-induced spin texture by performing fully spin-orbit coupled calculations. Figure 1(c) shows the electronic structures of 0°, 19.11° and 30° twisted graphene/WSe_2 heterostructures. We ob-

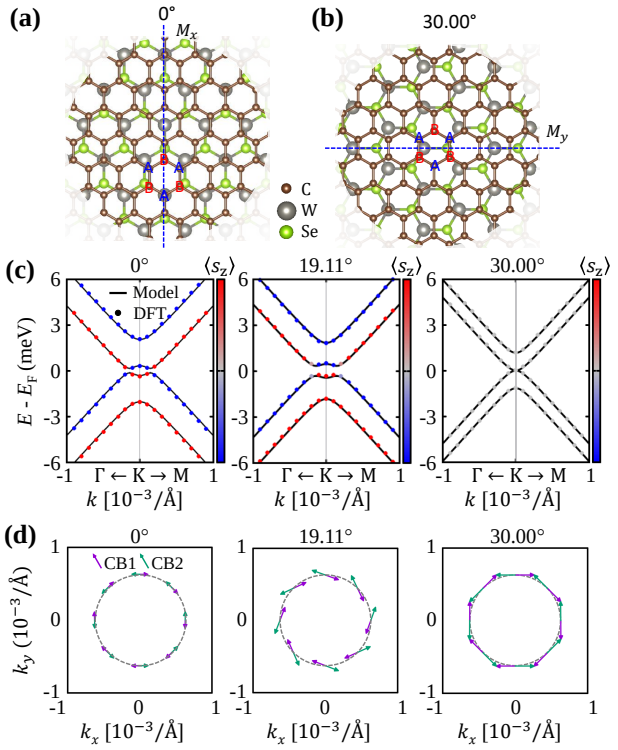

FIG. 1. Top views of graphene and WSe_2 heterostructure with (a) 0° and (b) 30° twist angles. In (a) and (b), the blue dashed lines indicate their corresponding mirror planes; and "A" and "B" highlight the sublattice sites of graphene. (c) Band structures and (d) in-plane spin distributions of the heterostructures with 0°, 19.11° and 30° twist angles. In (c), the colored dots indicate energy eigenvalues obtained by our DFT calculation, which were fitted by the model defined as the Eq. (1), plotted with the black solid lines. The color bar indicates the spin expectation value of its out-of-plane components. In (d), the purple and cyan arrows indicate the spins from the (CB1) lowest and (CB2) second lowest conduction bands.

serve well defined out-of-plane spin-polarized sub-bands and clearly inverted band structures for all $\theta \neq 30°$ twistings [37]. The in-plane spin textures for the three heterostructures are shown in Fig. 1(d). It exhibits a chiral Rashba-like spin-momentum locking superposed with an additional out-of-plane spin texture for all $\theta \neq 30°$, implying the existence of valley-Zeeman SOC [37]. Here, the spin states gradually tilt toward the in-plane direction with increasing θ, where $\langle s_z \rangle$ becomes completely quenched at 30° for all sub-bands. The removal of mirror plane symmetries at most twist angles also imbued the spin texture with additional features. Unlike ordinary Rashba spin splitted two-dimensional electron gas, herein, the in-plane spins are not perfectly orthogonal to the electrons momentum [26, 27].

To obtain the twist angle evolution of the proximity-induced SOC parameters, the band structure and spin texture were fitted to the continuum Hamiltonian [39]

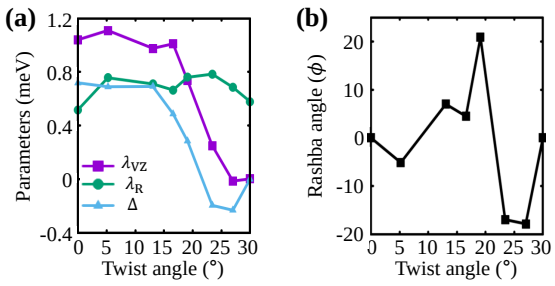

FIG. 2. The twist angle evolution of (a) parameters of model Hamiltonian as described in the Eq. (1) and (b) corresponding Rashba angle. In (a), purple, cyan, and skyblue lines indicate valley-Zeeman (λ_{VZ}), Rashba SOC (λ_R) and staggerd potential (Δ), respectively.

$$H(\kappa\mathbf{K}+\mathbf{k}) = \hbar v_F(\kappa\sigma_x k_x + \sigma_y k_y) + \Delta\sigma_z + \\ + \lambda_R e^{-is_z\phi/2}(\kappa\sigma_x s_y - \sigma_y s_x)e^{is_z\phi/2} + \\ + (\lambda_{VZ}\sigma_0 + \lambda_{KM}\sigma_z)\kappa s_z, \quad (1)$$

where v_F is the Fermi velocity in graphene, Δ is the sublattice asymmetry and $\kappa = \pm 1$ is the valley index (for valley $\pm\mathbf{K}$). The remaining parameters λ_R, λ_{VZ}, and λ_{KM} collectively account for the proximity-induced SOC and describe, respectively, the Rashba, valley-Zeeman, and Kane-Mele SOC terms. The last two terms also can be understood as antisymmetric and symmetric part of intrinsic SOC (λ_I) of two sublattices (A and B) of graphene, or $\lambda_{VZ} = (\lambda_I^A - \lambda_I^B)/2$, and $\lambda_{KM} = (\lambda_I^A + \lambda_I^B)/2$, respectively. Finally, the σ_i (s_i) matrices, with $i = 0, x, y, z$, operate on the orbital (spin) space and ϕ is the Rashba angle parameter accounting for the non-orthogonal spin-momentum locking [26–29]. Note that, as reported in earlier works [26–28], we also found λ_{KM} to be negligibly small and does not affect the CSC.

Figure 1(c) shows the excellent agreement between the first principles (symbols) and continuum model (solid) bands. The twist angle evolution of valley-Zeeman λ_{VZ}, λ_R and Δ are summarized in Fig. 2(a). We observe that λ_{VZ} is larger than λ_R at small twist angles, and both λ_{VZ} and Δ vanish at the 30° twist angle, as required by symmetries. This behavior is related to the existence of mirror planes in certain twisted graphene/WSe_2 systems and to the sublattice symmetry of graphene: Due to the C_6 and C_3 rotation symmetries of graphene and WSe_2, respectively, the 0° (30°)-twisted graphene/WSe_2 heterostructures possess a $\mathbf{M_x}$ ($\mathbf{M_y}$) mirror, as shown in Figs. 1(a) and (b), where we also highlight sublattice sites of graphene as "A" and "B". At $\theta = 0°$ ($\theta = 30°$) twisting, sublattices "A" and "B" are left (are not left) invariant under a $\mathbf{M_x}$ ($\mathbf{M_y}$) mirror operation. Hence, both λ_{VZ} and Δ vanish at $\theta = 30°$. In contrast, λ_R exhibits only a slight twist angle modulation, with a mag-

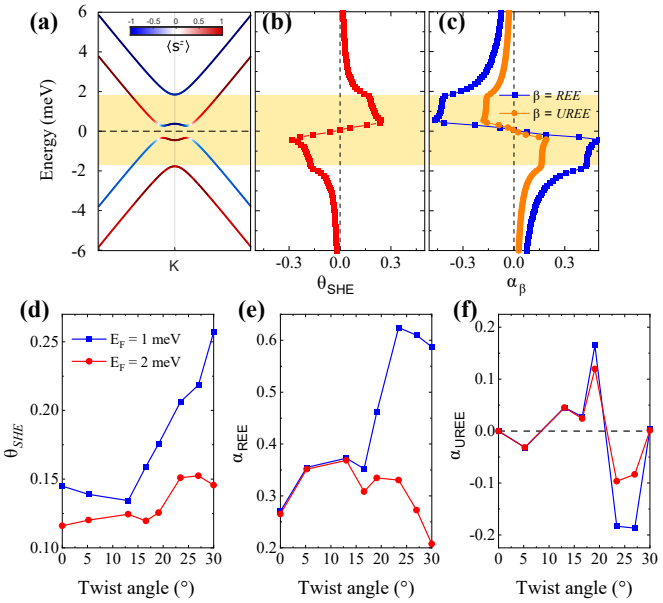

FIG. 3. (a) Spin-resolved band structure of a graphene/WSe_2 heterostructure with $\theta = 19.11°$. Colors refer to the $\langle s^z \rangle$ magnitude. The associated spin Hall, Rashba-Edelstein and unconventional Rashba-Edelstein efficiencies, $\theta_{\rm SHE}$, $\alpha_{\rm REE}$ and $\alpha_{\rm UREE}$ respectively, are shown in panels (b) and (c). The horizontal yellow stripes highlight the gap between conduction $\langle s^z \rangle = -1$ and valence $\langle s^z \rangle = +1$ sub-bands. The twist angle evolution of CSC efficiencies are displayed in panels (d), (e) and (f) at two distinct doping levels.

nitude that is approximately the same for both 0° and 30°. The twist angle evolution of the Rashba-angle, ϕ, is summarized in Fig. 2(b). The existence of $\mathbf{M_x}$ ($\mathbf{M_y}$) mirror planes constraints ϕ to be zero at 0° (30°) twisting [26, 27]. Symmetry breaking at all other twist angles enables the existence of finite ϕ. In addition, we find that the magnitude and sign of ϕ vary rapidly with the twist angle, resulting in the angle-dependent UREE, which will be discussed below.

Next, we study how the twist angle modulation of the proximity-induced SOC impacts CSC. As previously discussed, CSC in twisted graphene/WSe_2 is solely due to the proximitized Dirac cones at low doping levels. Hence, we write down a fully periodic tight-binding Hamiltonian to investigate the twist angle evolution of CSC. [37]. The electronic response to external electric fields is treated within the linear response theory. Here, we utilize the Kubo formula fashioned after Smrcka-Streda [40–43]:

$$\delta O^{\gamma}_{\alpha\beta} = \int \frac{d\mathbf{k}}{(2\pi)^2} [\delta O^{\gamma,I}_{\alpha\beta}(\mathbf{k}) + \delta O^{\gamma,II}_{\alpha\beta}(\mathbf{k})], \tag{2}$$

with integrands

$$\delta O^{\gamma,I}_{\alpha\beta}(\mathrm{k}) = -\frac{e\hbar}{\pi}\Gamma^2 \sum_{nm} \frac{\mathrm{Re}[\langle n\mathbf{k}|\hat{O}^{\gamma}_{\alpha}|m\mathbf{k}\rangle\langle m\mathbf{k}|\hat{v}_{\beta}|n\mathbf{k}\rangle]}{[(\epsilon_F - \epsilon_{n\mathbf{k}})^2 + \Gamma^2][(\epsilon_F - \epsilon_{m\mathbf{k}})^2 + \Gamma^2]}, \tag{3a}$$

$$\delta O^{\gamma,II}_{\alpha\beta}(\mathrm{k}) = -2e\hbar \sum_{n,m\neq n} (f_{n\mathbf{k}} - f_{m\mathbf{k}}) \frac{\mathrm{Im}[\langle n\mathbf{k}|\hat{O}^{\gamma}_{\alpha}|m\mathbf{k}\rangle\langle m\mathbf{k}|\hat{v}_{\beta}|n\mathbf{k}\rangle]}{(\epsilon_{n\mathbf{k}} - \epsilon_{m\mathbf{k}})^2 - \Gamma^2}, \tag{3b}$$

where $\hat{v}_\beta$ is the $\beta = x, y, z$ component of the velocity operator, $\hat{O}^{\gamma}_{\alpha}$ is the perturbed physical observable with spin index $\gamma = x, y, z$ and $|n\mathbf{k}\rangle$ is the eigenstate associated with the band $\epsilon_{n\mathbf{k}}$ of the unperturbed system. The Smrcka-Streda formula provides a good description in the weak disorder limit, which is assumed to only cause a constant band broadening quantified by Γ, and naturally includes both Fermi surface and Fermi sea contributions in Eqs. (3a) and (3b) respectively [40]. We note that disorder strongly impacts the SHE efficiency and leads to its cancellation in the Dirac-Rashba limit by virtue of covariant conservation laws [44]. While vertex corrections are fundamentally necessary to provide a realistic account of the CSC through the SHE in graphene/TMDC heterostructures, the disorder-free SHE calculations presented here can be used as reference in evaluating the potential of twist angle in modulating the SHE efficiency in the presence of disorder [13].

The charge, spin Hall and spin density responses are obtained through $\hat{O}^{\gamma}_{\alpha} \to -e\hat{v}_{\alpha}$, $\hat{O}^{\gamma}_{\alpha} \to (2/\hbar)\hat{Q}^{\gamma}_{\alpha}$, where the spin current operator is defined as $\hat{Q}^{\gamma}_{\alpha} = (1/2)\{\hat{s}^{\gamma}, \hat{v}_{\alpha}\}$ with spin operator $\hat{s}^{\gamma}$, and $\hat{O}^{\gamma}_{\alpha} \to \hat{s}^{\gamma}$, respectively. In the following, we assume a constant electric field applied along the $\hat{\mathbf{x}}$ direction and define the SHE, REE and UREE efficiencies as $\theta_{\rm SHE} = (2e/\hbar)\sigma^z_{yx}/\sigma_{xx}$, $\alpha_{\rm REE} = (2ev_F/\hbar)\delta s^y/\sigma_{xx}$ and $\alpha_{\rm UREE} = (2ev_F/\hbar)\delta s^x/\sigma_{xx}$, where σ^z_{yx} and σ_{xx} are the spin hall and charge conductivities, δs^y and δs^x are the electrically-induced spin densities, and $v_F = 1 \times 10^6$ m/s is the Fermi velocity in graphene [38].

Figure 3(a) shows the spin-resolved bands of 19.11° twisted graphene/WSe_2 at the vicinity of the K point. The associated energy-resolved SHE and REE efficiencies, shown in Figs. 3(b) and (c) considering $\Gamma = 0.1$ meV, reveal that efficient CSC takes place within a small energy window between the valence $\langle s^z \rangle = +1$ and conduction $\langle s^z \rangle = -1$ sub-bands [shaded yellow region in Figs. 3(a), (b) and (c)]. The presence of additional sub-bands at higher energies acts as to suppress the CSC due to their opposite contributions to the total spin-Berry curvature and opposite spin-momentum locking helicity. Figure 3(c) also shows a sizable UREE whose efficiency is comparable to the SHE. The observation of such novel spin currents, whose spin quantization axis and electric field direction are collinear, has been recently reported in the in graphene/$MoTe_2$ [45], graphene/WTe_2 [46], and graphene/$NbSe_2$ [47] heterostructures.

We explore the twist angle evolution of the CSC efficiencies at two distinct doping levels in Figs. 3(d), (e) and (f). Here, the maximum SHE efficiency for the higher doping case, $E_{\rm F} = 2$ meV, occurs between 23° and 27° twisting. The situation differs substantially at lower dop-

ing levels or $E_F = 1$ meV, where our results indicate a larger SHE efficiency at 30° twisting. Similar to the spin Hall case, the REE efficiency is also more sensitive to the twist angle at lower doping levels, as shown in Fig. 3(e). A similar behavior is observed for the UREE in Fig. 3(f). Remarkably, both REE and UREE become more efficient in the lowest doping case exhibiting a maximum at $\theta \approx 23°$ twisting. We also found that while the conventional REE efficiency remains sizable and finite at $\theta \approx 30°$, the UREE abruptly vanishes due to symmetry constraints on the Rashba angle ϕ with the restoration of a mirror plane. The absence of λ_{VZ} at 30° twisting suggests that the valley-Zeeman SOC is detrimental to the disorder-free SHE-based CSC efficiency in the clean limit. This is due to the fact that the charge conductivity σ_{xx} increases faster than σ^z_{yx} with λ_{VZ} [37].

Although SHE and REE CSC mechanisms are simultaneously present in graphene/WSe_2, their relative ability to produce spins might vary with doping, twist angle and disorder. For example, in the recent experiments, REE is dominant over SHE in WS_2/graphene/hBN/SiO_2/Si Hall bar devices [21], but the opposite is true in MoS_2 or WSe_2/graphene/SiO_2/Si devices [22, 23], which is consistent with the physical picture that REE dominates in the clean limit, as shown in Fig. 3. Here, we expect a disorder-induced crossover between CSC dominated by SHE and (U)REE, originating from the contrasting Fermi sea and Fermi surface nature of SHE and REEs, respectively. This is illustrated in Ref. [37], which sheds light on the disparate dominant CSC mechanism reported across different proximitized graphene Hall bar devices.

In summary, we have studied proximity effects and its relation to the charge-to-spin (CSC) conversion in twisted graphene/WSe_2 heterostructures from first principles. We have analysed in detail how the REE and disorder-free contribution to the SHE efficiencies are affected by the twist angle and found that optimal CSC occurs for structures with around 30° twisting. In addition, our results revealed that lack of mirror symmetry for $0° < \theta < 30°$ twisted structures leads to non-orthogonal Rashba spin texture, resulting in spin accumulation longitudinal to the applied electric field. Our work highlights the new physics of CSC in graphene/TMDC heterostructures brought about by twistronics.

Acknowledgments S. L. is primarily supported by Basic Science Research Program through the National Research Foundation of Korea funded by the Ministry of Education (NRF-2021R1A6A3A14038837). S. L. and T. L. are partially supported by NSF DMREF-1921629. D. S. and T. L. are partially supported by the Valleytronics Intel Science Technology Center, and SMART, one of the seven centers of nCORE, a Semiconductor Research Corporation program, sponsored by National Institute of Standards and Technology (NIST). Y.K. acknowledges financial support from the Korean government through the National Research Foundation of Korea (NRF-2022M3F3A2A01073562). Z.C. and F.C. acknowledge funding by the Valleytronics Intel Science Technology Center, the Spanish MICINN (Project RTI2018-094861-B-I00 and Maria de Maeztu Units of Excellence Programme CEX2020-001038-M) and by the Regional Council of Gipuzkoa (Project ORBILOGICS) F.J. acknowledges funding from the Spanish MCI/AEI/FEDER through grant PGC2018-101988-B-C21 and from Diputacion de Gipuzkoa through grant Gipuzkoa NEXT 2021-100-000070-01. We acknowledge the MSI in the University of Minnesota for providing the computational resources, and useful discussions with Raseong Kim and Ian Young from Intel Corporation. We thank Aires Ferreira and David T. S. Perkins for fruitful discussions on the vertex correction.

* These authors contributed equally to this work.
† tlow@umn.edu

[1] N. Tombros, C. Jozsa, M. Popinciuc, H. T. Jonkman, and B. J. van Wees, Nature **448**, 571 (2007).
[2] M. Drögeler, C. Franzen, F. Volmer, T. Pohlmann, L. Banszerus, M. Wolter, K. Watanabe, T. Taniguchi, C. Stampfer, and B. Beschoten, Nano Lett. **16**, 3533 (2016).
[3] W. Han, R. K. Kawakami, M. Gmitra, and J. Fabian, Nat. Nanotechnol. **9**, 794 (2014).
[4] J. Ingla-Aynés, R. J. Meijerink, and B. J. v. Wees, Nano Lett. **16**, 4825 (2016), ISSN 1530-6984.
[5] K. S. Novoselov, A. K. Geim, S. V. Morozov, D. Jiang, Y. Zhang, S. V. Dubonos, I. V. Grigorieva, and A. A. Firsov, Science **306**, 666 (2004).
[6] A. K. Geim and K. S. Novoselov, Nat. Mater. **6**, 183 (2007).
[7] J. H. Garcia, M. Vila, A. W. Cummings, and S. Roche, Chem. Soc. Rev. **47**, 3359 (2018).
[8] J. F. Sierra, J. Fabian, R. K. Kawakami, S. Roche, and S. O. Valenzuela, Nat. Nanotechnol. **16**, 856868 (2021).
[9] A. Avsar, H. Ochoa, F. Guinea, B. Özyilmaz, B. J. van Wees, and I. J. Vera-Marun, Rev. Mod. Phys. **92**, 021003 (2020).
[10] M. Gmitra and J. Fabian, Phys. Rev. B **92**, 155403 (2015).
[11] M. Gmitra, D. Kochan, P. Högl, and J. Fabian, Phys. Rev. B **93**, 155104 (2016).
[12] Z. Wang, D.-K. Ki, H. Chen, H. Berger, A. H. MacDonald, and A. F. Morpurgo, Nat. Commun. **6**, 8339 (2015).
[13] J. H. Garcia, A. W. Cummings, and S. Roche, Nano Lett. **17**, 5078 (2017).
[14] B. Yang, M.-F. Tu, J. Kim, Y. Wu, H. Wang, J. Alicea, R. Wu, M. Bockrath, and J. Shi, 2D Mater. **3**, 031012 (2016).
[15] S. Zihlmann, A. W. Cummings, J. H. Garcia, M. Kedves, K. Watanabe, T. Taniguchi, C. Schönenberger, and P. Makk, Phys. Rev. B **97**, 075434 (2018).
[16] T. Wakamura, F. Reale, P. Palczynski, S. Guéron, C. Mattevi, and H. Bouchiat, Phys. Rev. Lett. **120**, 106802 (2018).
[17] A. W. Cummings, J. H. Garcia, J. Fabian, and S. Roche,

Phys. Rev. Lett. **119**, 206601 (2017).
[18] T. S. Ghiasi, J. Ingla-Ayns, A. A. Kaverzin, and B. J. van Wees, Nano Lett. **17**, 7528 (2017).
[19] L. A. Benítez, J. F. Sierra, W. Savero Torres, A. Arrighi, F. Bonell, M. V. Costache, and S. O. Valenzuela, Nat. Phys. **14**, 303 (2018).
[20] J. Ingla-Aynés, F. Herling, J. Fabian, L. E. Hueso, and F. Casanova, Phys. Rev. Lett. **127**, 047202 (2021).
[21] T. S. Ghiasi, A. A. Kaverzin, P. J. Blah, and B. J. van Wees, Nano Lett. **19**, 5959 (2019).
[22] C. K. Safeer, J. Ingla-Ayns, F. Herling, J. H. Garcia, M. Vila, N. Ontoso, M. R. Calvo, S. Roche, L. E. Hueso, and F. Casanova, Nano Lett. **19**, 1074 (2019).
[23] F. Herling, C. K. Safeer, J. Ingla-Ayns, N. Ontoso, L. E. Hueso, and F. Casanova, APL Mater. **8**, 071103 (2020).
[24] L. A. Bentez, W. Savero Torres, J. F. Sierra, M. Timmermans, J. H. Garcia, S. Roche, M. V. Costache, and S. O. Valenzuela, Nat. Mater. **19**, 170175 (2020).
[25] L. Li, J. Zhang, G. Myeong, W. Shin, H. Lim, B. Kim, S. Kim, T. Jin, S. Cavill, B. S. Kim, et al., ACS Nano **14**, 5251 (2020).
[26] Y. Li and M. Koshino, Phys. Rev. B **99**, 075438 (2019).
[27] A. David, P. Rakyta, A. Kormányos, and G. Burkard, Phys. Rev. B **100**, 085412 (2019).
[28] T. Naimer, K. Zollner, M. Gmitra, and J. Fabian, Phys. Rev. B **104**, 195156 (2021).
[29] A. Pezo, Z. Zanolli, N. Wittemeier, P. Ordejón, A. Fazzio, S. Roche, and J. H. Garcia, 2D Mater. **9**, 015008 (2021).
[30] A. Veneri, D. T. S. Perkins, C. G. Péterfalvi, and A. Ferreira, Phys. Rev. B **106**, L081406 (2022).
[31] C. G. Péterfalvi, A. David, P. Rakyta, G. Burkard, and A. Kormányos, Phys. Rev. Research **4**, L022049 (2022).
[32] W. Kohn and L. J. Sham, Phys. Rev. **140**, A1133 (1965).
[33] G. Kresse and J. Furthmüller, Phys. Rev. B **54**, 11169 (1996).
[34] Z. Wang, Q. Chen, and J. Wang, J. Phys. Chem. C **119**, 4752 (2015).
[35] A. N. Kolmogorov and V. H. Crespi, Phys. Rev. B **71**, 235415 (2005).
[36] S. Singh, C. Espejo, and A. H. Romero, Phys. Rev. B **98**, 155309 (2018).
[37] See Supplemental Material at for details for DFT and transport calculations, and crystal and electronic structures, Rashba angles, and charge to spin conversion results of all twist angles, Supplemental Notes S1-S2, Supplemental Table S1, and Supplemental Figs. S1S7.
[38] M. Offidani, M. Milletarì, R. Raimondi, and A. Ferreira, Phys. Rev. Lett. **119**, 196801 (2017).
[39] D. Kochan, S. Irmer, and J. Fabian, Phys. Rev. B **95**, 165415 (2017).
[40] J. Železný, Y. Zhang, C. Felser, and B. Yan, Phys. Rev. Lett. **119**, 187204 (2017).
[41] H. Li, H. Gao, L. P. Zârbo, K. Výborný, X. Wang, I. Garate, F. Doğan, A. Čejchan, J. Sinova, T. Jungwirth, et al., Phys. Rev. B **91**, 134402 (2015).
[42] V. Bonbien and A. Manchon, Phys. Rev. B **102**, 085113 (2020).
[43] F. Freimuth, S. Blügel, and Y. Mokrousov, Phys. Rev. B **90**, 174423 (2014).
[44] M. Milletarí, M. Offidani, A. Ferreira, and R. Raimondi, Phys. Rev. Lett. **119**, 246801 (2017).
[45] C. K. Safeer, N. Ontoso, J. Ingla-Aynés, F. Herling, V. T. Pham, A. Kurzmann, K. Ensslin, A. Chuvilin, I. Robredo, M. G. Vergniory, et al., Nano Lett. **19**, 8758 (2019), ISSN 1530-6984.
[46] L. Camosi, J. Světlík, M. V. Costache, W. S. Torres, I. F. Aguirre, V. Marinova, D. Dimitrov, M. Gospodinov, J. F. Sierra, and S. O. Valenzuela, 2D Mater. **9**, 035014 (2022).
[47] J. Ingla-Aynés, I. Groen, F. Herling, N. Ontoso, C. K. Safeer, F. de Juan, L. E. Hueso, M. Gobbi, and F. Casanova, 2D Mater. **9**, 045001 (2022).